Preparation and characterization of inorganic radioactive holmium-166 microspheres for internal radionuclide therapy

A.G. Arranja[a,b,c], W.E. Hennink[a], C. Chassagne[d], A.G. Denkova[b], J.F.W. Nijsen[c,e,*]

[a] *Department of Pharmaceutics, Utrecht Institute for Pharmaceutical Sciences (UIPS), Science for Life, Faculty of Science, Utrecht University, 3508 TB, Utrecht, the Netherlands*
[b] *Radiation Science and Technology, Delft University of Technology, Mekelweg 15, 2629 JB, Delft, the Netherlands*
[c] *Radboudumc, Department of Radiology and Nuclear Medicine, Geert Grooteplein Zuid 10, 6525 GA, Nijmegen, the Netherlands*
[d] *Department of Hydraulic Engineering, Delft University of Technology, Stevinweg 1, 2628 CN, Delft, the Netherlands*
[e] *Quirem Medical B.V, Zutphenseweg 55, 7418 AH, Deventer, the Netherlands*

A B S T R A C T

Microspheres with high specific activities of radionuclides are very interesting for internal radiotherapy treatments. This work focuses on the formulation and characterization of inorganic microspheres with a high content of holmium and therefore a high specific radioactivity of holmium-166. Two novel formulations of inorganic microspheres were obtained by dispersing solid holmium acetylacetonate microspheres ($Ho_2(AcAc)_3$-ms) in NaH_2PO_4 or $NaOH$ solutions followed by 2 h incubation at room temperature. By exchange of acetylacetonate with phosphate or hydroxyl ions, holmium phosphate microspheres ($HoPO_4$-ms) and holmium hydroxide microspheres ($Ho(OH)_3$-ms) were formed respectively. The inorganic microspheres had a significantly smaller diameter (28.5 ± 4.4 μm ($HoPO_4$-ms) and 25.1 ± 3.5 μm ($Ho(OH)_3$-ms)) than those of $Ho_2(AcAc)_3$-ms (32.6 ± 5.2 μm). The weight percentage of holmium-165 in the microspheres increased significantly from 47% ($Ho_2(AcAc)_3$-ms) to 55% ($HoPO_4$-ms) and 73% ($Ho(OH)_3$-ms). After preparation of both $HoPO_4$-ms and $Ho(OH)_3$-ms, the stable holmium-165 isotope was partly converted by neutron activation into radioactive holmium-166 to yield radioactive microspheres. High specific activities were achieved ranging from 21.7 to 59.9 MBq/mg ($^{166}HoPO_4$-ms) and from 28.8 to 79.9 MBq/mg ($^{166}Ho(OH)_3$-ms) depending on the neutron activation time. The structure of both microspheres was preserved up to neutron activations of 6 h in a thermal neutron flux of 4.72×10^{16} n m^{-2} s^{-1}. After activation, both microspheres revealed excellent stability in administration fluids (saline and phosphate buffer) having less than 0.05% of holmium released after 72 h incubation. Finally, the hemocompatibility of these inorganic microspheres was evaluated and it was shown that the microspheres did cause neither hemolysis nor depletion or inhibition of the coagulation factors of the intrinsic blood coagulation pathway meaning that the microspheres have a good hemocompatibility. Overall, this work shows that radioactive inorganic microspheres with high specific activities of holmium-166 can be prepared which potentially can be used for internal radionuclide therapy.

1. Introduction

Liver cancer is one of the most aggressive tumor types with severe morbidity and high mortality rates. In 2012, it was the fifth most common cancer type and accounted for 9.1% (approximately 700 000 people) of all cancer related deaths in the world [1–4]. Moreover, the rates of liver cancer have consistently been increasing over the past years with 3% per year since the year 2000 (American Cancer Society). Therefore, liver cancer remains an important public health issue.

The therapies available for liver cancer patients and the selection of treatments depend on a wide range of characteristics such as the number, size and location of the tumor(s), the tumor stage at diagnosis and the patient's age. Surgery (partial hepatectomy) is the first option but only 15% of the patients can benefit from this treatment achieving a 5-year survival ranging from 25 to 51% [5]. For unresectable liver cancers, other treatments are available such as ablation, immunotherapy, chemotherapy and radiotherapy [2,5]. In particular, there have been major developments in the field of internal radionuclide therapy. Currently, different treatment modalities are being used with good safety profiles and efficacy such as segmental ablative

transarterial radioembolization (or radiation segmentectomy) [6], selective internal radiation therapy (SIRT) [7,8] and direct intratumoral injection (or interstitial microbrachytherapy) [9–14]. The main goal of these radionuclide therapies is to locally deliver tumoricidal doses of radiation to the tumors leaving healthy liver tissue unharmed [15–21]. These therapies are commonly performed using radioactive microspheres which contain radioisotopes emitting high-energy beta-minus (β^-) particles [14,19,22] such as yttrium-90 (^{90}Y) [23–25], holmium-166 (^{166}Ho) [26,27], phosphorous-32 (^{32}P) [24,28], iodine-131 (^{131}I) [29] and rhenium-188 (^{188}Re) [30]. So far, three formulations of radioactive microspheres have reached the market and are currently being clinically used for selective internal radiation therapy (SIRT) of liver malignancies: QuiremSpheres® [31], SIR-Spheres® [32] and TheraSphere® [33].

A critical factor for the success of these treatments is an appropriate administration of the microspheres and treatment follow-up which can only be achieved using imaging and quantification techniques during and after administration of the microspheres. The clinically utilized SIR-Spheres® and TheraSphere® contain ^{90}Y as a radionuclide which is a pure β^- emitter with no gamma rays for imaging and no magnetic or paramagnetic properties. Using ^{90}Y-based microspheres makes imaging of the microspheres very challenging [19]. The QuiremSpheres® (radioactive ^{166}Ho-loaded poly(lactic acid) microspheres) (^{166}Ho-PLA-ms) are the only product that enables visualization and quantification of the microspheres during and after administration of the microspheres based on high resolution magnetic resonance imaging (MRI) and computer tomography (CT) [34–37]. The QuiremSpheres® are composed of poly(lactic acid), acetylacetonate and ^{165}Ho that, after thermal neutron capture, is converted into the radioactive ^{166}Ho (^{165}Ho + n → ^{166}Ho) [38,39]. This isotope does not only emits β^- particles, which destroy the tumor cells, but it also emits low-energy gamma photons (6.2% 81 keV, 0.93% 1.38 keV) enabling visualization by single-photon emission computed tomography (SPECT) [35,40,41]. Holmium has also a high attenuation coefficient and paramagnetic properties which allows its visualization by CT and MRI [35,36,42].

Moreover, due to the fact that the ^{166}Ho-PLA-ms can be easily imaged using conventional imaging techniques, the use of the same microspheres as "scout dose" (QuiremScout® [43]) based on the same type of microspheres (equal density, size and morphology, but at a lower dose) gives the possibility to better predict the distribution of the treatment dose and avoid unwanted extrahepatic deposition of the microspheres during the SIRT procedure [44–46]. Therefore, using the same type of microspheres for the "scout dose" and the treatment is more predictable on the therapeutic microsphere's distribution than the commonly used gamma-emitter tracer technetium-99 m albumin macroaggregates (^{99m}Tc-MAA) [45,47,48].

The ^{166}Ho-PLA-ms have a mean holmium content of 19 wt% and a maximum ^{166}Ho specific activity of 450 Bq/microsphere under optimized neutron activation conditions [19]. It is highly attractive to develop microspheres with higher holmium content in order to achieve higher specific activities. The higher holmium content and specific activity has major advantages regarding the imaging and quantification performance of the microspheres (SPECT, MRI and CT) [8,36]. The elevated activity also provides an increased time for transportation that simplifies the logistics handling of the products from the neutron activation facility (nuclear reactor) to the hospital (t$_{1/2}$ ^{166}Ho = 26.8 h). Furthermore, it also enables the administration of lower volumes of radioactive formulation and makes other potential clinical applications feasible such as radiation segmentectomy and interstitial microbrachytherapy because smaller doses of microspheres containing a high specific activity can be used for these applications [14,49].

In previous work of our group, the development of microspheres with a much higher holmium content of ~ 47 wt% than the current clinically used ^{166}Ho-PLA-ms ([Ho] = ~ 19 wt%) was reported [26,27,50,51]. These microspheres composed of holmium acetylacetonate (Ho$_2$(AcAc)$_3$-ms) can achieve higher specific activities than

the ^{166}Ho-PLA-ms and are converted into holmium phosphate microspheres after neutron activation up on incubation in phosphate buffer [26]. Although this is a major improvement in terms of specific radioactivity per gram of microspheres, there is still room for particles with a higher specific activity. Therefore, the aim of this work is to develop microspheres with higher holmium content than our recently published Ho$_2$(AcAc)$_3$-ms ([Ho] = ~ 47 wt%). The microspheres also need to be stable in administration fluids after neutron activation and be compatible with human blood. According to the ISO 10993–1:2018 requirements (Biological evaluation of medical devices), the compatibility of the microspheres with human blood is of utmost importance as this is the first biological interaction of the medical device with the patient.

This work is therefore focused on the development of inorganic microspheres due to the possibility to achieve high metal content per weight. Two formulations of microspheres comprising holmium inorganic complexes were developed, namely holmium phosphate microspheres (HoPO$_4$-ms) and holmium hydroxide microspheres (Ho(OH)$_3$-ms). Both inorganic formulations were obtained using the previously developed Ho$_2$(AcAc)$_3$-ms as their precursor [26,27,50,51]. The new inorganic microspheres were neutron activated for different times and the specific activities as well as the stability of the microspheres in common administration fluids were investigated. Finally, the hemocompatibility (hemolysis and coagulation) of the microspheres was tested in human blood.

2. Materials and methods

2.1. Materials

Holmium chloride (HoCl$_3$.6H$_2$O; product code 6735, MW 379.38; 99.9%) was obtained from Metall Rare Earth Limited (Shenzhen, China). Acetylacetone (AcAc; ReagentPlus®; MW 100.12; > 99%), polyvinyl alcohol (PVA; MW 30.000–70.000; 87–90% hydrolyzed), holmium oxide (Ho$_2$O$_3$; MW 377.86; 99.999%), sodium phosphate monobasic anhydrous (NaH$_2$PO$_4$, MW 119.98; > 99.0%), sodium phosphate dibasic dihydrate (Na$_2$HPO$_4$.2H$_2$O, MW 177.99; > 98.5%), lyophilized powder of human hemoglobin (H7379), Dulbecco's Phosphate Buffered Saline Ca^{2+}/Mg^{2+}-free (DPBS, D8537),Triton X-100 solution (BioUltra, 10% in H$_2$O, 93443), anhydrous calcium chloride (CaCl$_2$, C1016), sodium hydroxide (NaOH, pellets EMPLURA®, 1064621000), ammonium hydroxide (NH$_4$OH 28–30%, 221228), chloroform (CHCl$_3$, EMPROVE®, 1024311000), nitric acid (HNO$_3$ 70%, 438073), holmium ICP standard (1000 mg/l, Certipur®) and phosphorous ICP standard (1000 mg/l, Certipur®) were supplied by Merck-Millipore (Darmstadt, Germany). Absolute methanol was supplied by Biosolve (Valkenswaard, the Netherlands) and perchloric acid (70%) by ACROS Organics (Geel, Belgium). The 0.9% sodium chloride solution (Mini-Plasco NaCl) was supplied by B.Braun Medical (Diegem, Belgium). Pharmaceutical grade powder of kaolin was purchased from BDH ltd (Poole, UK). Dade Actin FS Activated PTT Reagent was purchased from Siemens Healthcare (Erlangen, Germany). The Cyanmethemoglobin (CMH) reagent or Drabkin's solution (D5941) was obtained from Sigma-Aldrich Chemie N.V. (Zwijndrecht, the Netherlands).

2.2. Methods

2.2.1. Preparation of Ho$_2$(AcAc)$_3$. HoPO$_4$ and Ho(OH)$_3$ microspheres

The starting material to prepare the HoPO$_4$ and Ho(OH)$_3$ microspheres was Ho$_2$(AcAc)$_3$ microspheres Ho$_2$(AcAc)$_3$-ms) (Fig. 1-A,B) prepared as previously reported [26,27,50]. Briefly, crystals of holmium acetylacetonate (10 g) [52] were dissolved in chloroform (186 g) and this solution was added to an aqueous solution of polyvinyl alcohol (1 L water with 2% w/w PVA). Overhead four blades propeller stirrers (Hei-TORQUE Value 100, Heidolph, Germany) were used to vigorously stir the mixture at 300 rpm in 2 L baffled beakers to obtain an oil-in-
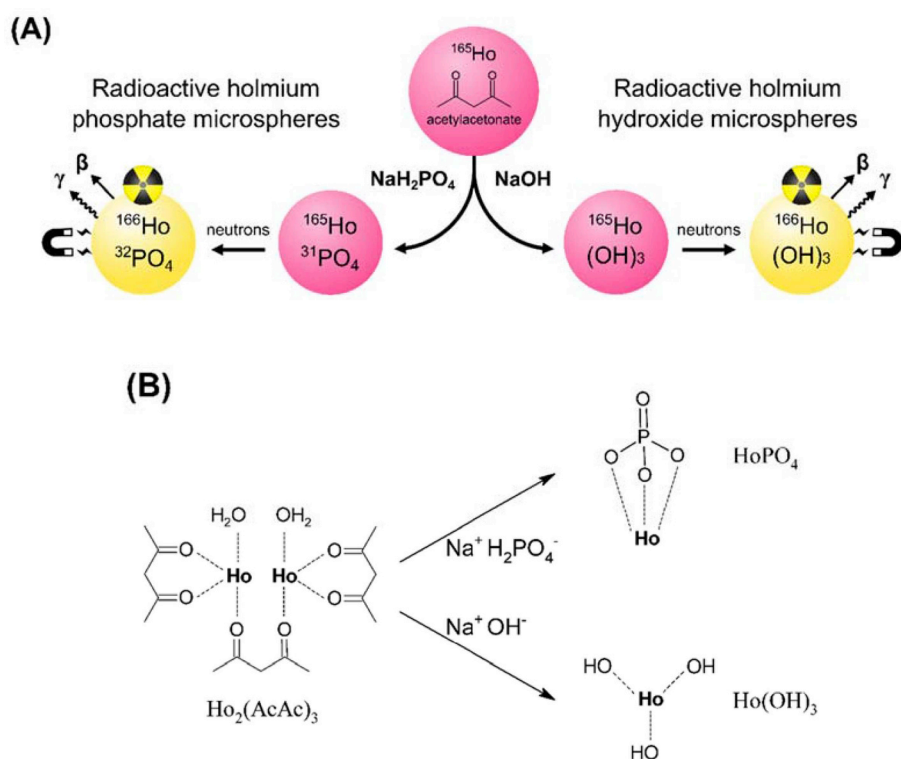
Fig. 1. (A) Schematic overview of the steps to prepare radioactive holmium phosphate microspheres (HoPO$_4$-ms) and holmium hydroxide microspheres (Ho(OH)$_3$-ms). Holmium acetylacetonate microspheres (Ho$_2$(AcAc)$_3$-ms) were incubated in sodium phosphate (NaH$_2$PO$_4$) or sodium hydroxide (NaOH) solutions for 2 h at room temperature to yield HoPO$_4$-ms or Ho(OH)$_3$-ms respectively, followed by neutron activation to generate radioactive microspheres. (B) Representation of the chemical structures of Ho$_2$(AcAc)$_3$-ms, and the HoPO$_4$-ms and Ho(OH)$_3$-ms upon incubation with NaH$_2$PO$_4$ or NaOH solutions.

water (o/w) emulsion. Stirring was continued at 25 °C and a constant flow of nitrogen gas (12 L/min) was applied for 72 h to allow evaporation of chloroform. Next, the microspheres dispersed in the PVA/water phase were sieved according to the desired size (20–50 μm) using an electronic sieve vibrator (TOPAS EMS 755). Finally, the sieved microspheres were vacuum dried at room temperature for 72 h.

The dried Ho$_2$(AcAc)$_3$-ms (7 g) were added to aqueous solutions of 525 mL sodium phosphate monobasic (36.5 g NaH$_2$PO$_4$, 0.58 M, pH 4.2) or 875 mL sodium hydroxide (17.5 g NaOH, 0.50 M, pH 13.5) to form HoPO$_4$ or Ho(OH)$_3$ microspheres respectively. The dispersion was prepared in 2 L baffled beakers and continuously stirred at 500 rpm for 2 h using overhead four blades propeller stirrers (Hei-TORQUE Value 100, Heidolph, Germany) at room temperature (20–25 °C). After stirring, the formed HoPO$_4$ or Ho(OH)$_3$ microspheres were collected into four 50 mL tubes. The microspheres were washed four times with water followed by centrifugation. After washing, the microspheres were dried in a vacuum oven at room temperature for 24 h.

The formation kinetics of the HoPO$_4$-ms or Ho(OH)$_3$ was determined by High Performance Liquid Chromatography (HPLC) analysis by measuring the acetylacetone released from the microspheres in the supernatant at different time points. Samples of the supernatant were analyzed using an Alliance HPLC system equipped with a C18 column (XSelect CSH C18 3.5 μm 4.6 × 150 mm, Waters) at 40 °C and a 70:30 mixture of methanol:water with 0.1% perchloric acid as the mobile phase (0.5 mL/min). Detection of the acetylacetone was performed at 280 nm. The hydrolysis rate of acetylacetone in alkaline solution was also studied by incubation of pure acetylacetone in 0.5 M NaOH (3.5 mg of acetylacetone per mL of NaOH solution) and analysis of this solution by HPLC over a period of 24 h.

2.2.2. Characterization of Ho$_2$(AcAc)$_3$, HoPO$_4$ and Ho(OH)$_3$ microspheres

The size distributions of the Ho$_2$(AcAc)$_3$-ms and the HoPO$_4$-ms and Ho(OH)$_3$-ms were determined using a Coulter counter equipped with an orifice of 100 μm (Multisizer 3, Beckman Coulter, Mijdrecht, the Netherlands). An optical microscope (AE2000 Motic) was used to investigate the morphological properties of the microspheres suspended in water (sphericity and surface damages). The surface composition and smoothness of the microspheres was analyzed using a Scanning Electron Microscope-Energy Dispersive X-ray Spectroscopy (SEM-EDS) (JEOL JSM-IT100, InTouchScope™, Tokyo, Japan).

The zeta potential of the HoPO$_4$-ms or Ho(OH)$_3$-ms microspheres was determined using a ZetaCompact (CAD instruments, France). The samples were prepared by dispersing approximately 50 mg of microspheres in 10 mL of water for injection (BBraun, Germany). The pH's of the dispersions were measured (FiveEasy Plus, Mettler Toledo LE410) and were 7.3 ± 0.2 for the HoPO4-ms and 7.0 ± 0.1 for the Ho(OH)3-ms (n = 3 for each microsphere type). The samples were transferred into a quartz capillary cell and the electrophoretic mobility of individual microspheres was recorded by video microscopy. The zeta potential was then obtained using the Smoluchowski formula [53]. The zeta potential of 500–1000 microspheres of HoPO$_4$ and of Ho(OH)$_3$ was obtained.

The density of the HoPO$_4$-ms and Ho(OH)$_3$-ms was determined in water using a 25 cm^3 specific gravity bottle (Blaubrand NS10/19, DIN ISO 3507, Wertheim, Germany) and using a sample amount of approximately 250 mg.

The holmium (Ho) and phosphorous (P) contents were determined by Inductively Coupled Plasma-Optical Emission spectroscopy (ICP-OES). Before preparation of the samples for ICP-OES analysis, the microspheres were dried overnight in a vacuum oven at room temperature. Then, samples of 20–50 mg were dissolved in 50 mL of 2% nitric acid and the Ho concentration of the solutions was measured at three different wavelengths (339.9, 345.6 and 347.4 nm) and the P concentration at two wavelength (213.6 and 214.9 nm) using an Optima 4300 CV (PerkinElmer, Norwalk, USA). The calibration solutions for the ICP-OES measurements were prepared by dissolving holmium or phosphorous ICP standards in 2% nitric acid in concentrations ranging from 0.001 mg/L to 75 mg/L.

The Ho content was also determined by Atomic Absorption Spectroscopy (PerkinElmer Model AAnalyst 200) and the carbon (C) and hydrogen (H) contents determined with a CHNS analyzer (Elementar Model Vario Micro Cube). These elemental determinations of the Ho, C and H contents were performed in duplicate by Mikroanalytisches Laboratorium KOLBE (Oberhausen, Germany) and

the samples were dried overnight in a vacuum oven at 100 °C. The oxygen (O) content could not be determined accurately due to interference of holmium, and was assumed to be the remaining component on the microspheres as no other element is expected to be present [% O = 100 − (%C + %H + %P + %Ho)].

X-ray powder diffraction (XRD) patterns of the $HoPO_4$-ms and Ho$(OH)_3$-ms were obtained by depositing a small amount (around 5 mg) of each sample on a Si-510 wafer and analyzed using a Bruker D8 Advance diffractometer in Bragg-Brentano geometry with a Lynxeye position sensitive detector.

Fourier transform infrared (FTIR) spectra of the $HoPO_4$-ms and Ho$(OH)_3$-ms were recorded using a Nicolet 8700 FTIR spectrometer (Thermo Electron Corporation) equipped with a KBr/DLaTGS D301 detector cooled with liquid nitrogen. A small amount of each sample (5–10 mg) was pressed onto KBr salts and the sample holder was stabilized for 5 min at 25 °C and kept at this temperature during the analysis. The FTIR spectra of the microspheres were recorded at a resolution of 4 cm^{-1} averaged over 128 scans.

Thermogravimetric analysis (TGA) of the microspheres was performed using a TGA2 Star System (Mettler Toledo). Samples of 12–15 mg of microspheres were heated from 30 up to 800 °C under a nitrogen atmosphere at a heating rate of 5 °C/min and the weight loss was recorded. Before weighting the samples, the microspheres were dried overnight in a vacuum oven at 100 °C. After the treatment, the resulting powders were also analyzed by FTIR using the same conditions as described above.

2.2.3. Neutron activation of $HoPO_4$ and Ho$(OH)_3$ microspheres

The $HoPO_4$-ms and Ho$(OH)_3$-ms were neutron activated in the pneumatic rabbit system (PRS) facility of the nuclear reactor research facility (HOR, Hoger Onderwijs Reactor) operational at the Department of Radiation Science and Technology of the Delft University of Technology, the Netherlands. This facility has an average neutron thermal flux of 4.72×10^{16} n $m^{-2} s^{-1}$, epithermal neutron flux of 7.87×10^{14} n $m^{-2} s^{-1}$ and a fast neutrons flux of 3.27×10^{15} n $m^{-2} s^{-1}$. Different weights of microspheres (from 251 to 292 mg) were sealed in polyethylene vials which were placed into polyethylene rabbits for neutron activation [47,54]. The microspheres were activated for 2, 4 and 6 h (n = 2) to yield radioactive $^{166}Ho^{32}PO_4$-ms and $^{166}Ho$$(OH)_3$-ms (Fig. 1-A). Upon neutron activation of the $HoPO_4$-ms, besides the formation of ^{166}Ho, also the element phosphorus is neutron activated to yield radioactive ^{32}P ($^{31}P + n \rightarrow {}^{32}P$). The expected activity at the end of neutron activation ($A_{EoA,expected}$) can be determined for each isotope using Equations (1) and (2). The nuclear data related to the elements used in this study including the cross-section for thermal neutrons are shown in Table S1.

$$A_{EoA,\ expected} = \sigma \ . \ \varphi \ . \ N \ (1 - e^{-\lambda t}) \tag{1}$$

$$N = \frac{m}{M_w} . \ \theta \ . \ N_A \tag{2}$$

where:

σ cross-section for thermal neutrons (barns = 10^{-24} cm^2)
φ thermal neutron flux (n/cm^2s)
    N = number of parent atoms
    m = mass of element in the sample
    M_w = molecular weight of the element
θ isotopic abundance
    N_A = avogadro constant
λ decay constant (s^{-1})
    t = irradiation time (s)

After neutron activation, the activity of the samples at a specific time (A_t) was measured using a dose calibrator (VDC-603, Comecer, the Netherlands). The activity of the samples ($HoPO_4$-ms and Ho$(OH)_3$-ms)

was measured when the activity was between 200 and 600 MBq/sample, which corresponds to 6–8 days after neutron activation. The activity in the $HoPO_4$-ms samples was measured when the activity of ^{32}P had a contribution of less than 1% to the total activity, which was less than 8 days after neutron activation. This measurement enables the calculation of the activity at the end of neutron activation (A_{EoA}) by taking into account the nuclide radioactive decay after neutron activation and the time at which the microspheres were analyzed for radioactive measurement, according to the following equations:

$$A_t = A_{EoA} \ . \ e^{-\lambda t} \tag{3}$$

$$\lambda = \frac{\ln 2}{t_{1/2}} \ , \lambda \ = \ \text{decay constant (s}^{-1}) \text{ and } t_{1/2}$$

$$= \ \text{half} - \text{life of the radionuclide} \tag{4}$$

2.2.4. Stability of microspheres in administration fluids after neutron activation

The stability of non-radioactive microspheres in administration fluids was evaluated by incubation of non-radioactive $HoPO_4$-ms and Ho$(OH)_3$-ms in 0.116 M phosphate buffer (0.077 M $Na_2HPO_4.2H_2O$ + 0.039 M NaH_2PO_4, pH 7.2) and 0.9% NaCl (300 mg of microspheres in 2 mL). After adding the administration fluids, the suspensions were vortexed for 10 min and samples were collected after 24 and 48 h to analyze the morphological properties of the microspheres using an optical microscope (method described in section 2.2.2.).

The stability of the $HoPO_4$-ms and Ho$(OH)_3$-ms after neutron activation was tested after decay of the radioactive ^{166}Ho for more than 20 days (after more than 18 half-life's) to minimize personnel radiation exposure. Then, 2 mL of 0.116 M phosphate buffer (composition given in previous paragraph) was added to each vial containing neutron activated $HoPO_4$-ms and 2 mL of 0.9% NaCl were added to each vial containing neutron activated Ho$(OH)_3$-ms. After adding the administration fluids, the suspensions were vortexed for 10 min. Then, at predetermined time points (1, 24, 48 and 72 h), samples of the suspensions were collected and the morphological properties of the microspheres were observed by optical microscopy and size distributions determined (methods described in section 2.2.2.). Samples of the supernatant (200 μL) were collected at the same time points after centrifugation (2000×g, 10 min), diluted in 5 mL of 2% nitric acid and analyzed by ICP-OES to detect possible holmium leakage (method described in section 2.2.2.).

2.2.5. Hemocompatibility
2.2.5.1. Incubation with full blood.
Blood from healthy volunteers was collected in sodium heparin blood tubes (Vacuette NH Sodium Heparin, Greiner bio-one, North Carolina, USA). On the same day of blood collection, 900 μL of blood was added to 100 μL of suspensions of $HoPO_4$-ms or Ho$(OH)_3$-ms dispersed in 0.9% NaCl at final concentrations of 0, 5, 10, 20 and 40 mg/mL (n = 3). The blood containing the dispersed microspheres was immediately incubated at 37 °C with gentle mixing (VWR nutating mixer). After incubation, blood samples of 160 μL were collected at predetermined time points (4 and 24 h). The blood hemogram (white blood cell count and viability, red blood cell count, red cell distribution width, mean corpuscular volume, mean corpuscular hemoglobin concentration and hematocrit) was obtained at 4 and 24 h incubating time using an automated blood cell analyzer (Cell-Dyn sapphire, Abbott Diagnostics, Santa Clara, CA, USA). Experiments were performed in triplicate. The statistical analysis of the results was carried out by two-way ANOVA (*p < 0.05) using Origin 9 software.

2.2.5.2. Coagulation.
For the coagulation assay, blood from healthy volunteers was anticoagulated with sodium citrate (BDVacutainer®, 0.105 M Na_3Citrate). Platelet-poor plasma (PPP) was isolated by centrifugation of the blood at 20–22 °C (2500×g, 10 min). Then,

675 μL of PPP was added to Eppendorf tubes containing 75 μL of $HoPO_4$-ms or $Ho(OH)_3$-ms suspensions (dispersed in in 0.9% NaCl) at final concentrations of 0.04, 0.2, 1 and 10 mg/mL (n = 3). The vehicle (0.9% NaCl) was also tested by adding 675 μL of PPP to Eppendorf tubes containing 75 μL of 0.9% NaCl without microspheres. As negative control, only PPP was added to the Eppendorf tubes (n = 3). As positive control, 675 μL of PPP was added to Eppendorf tubes containing 75 μL of kaolin suspension to achieve a final concentration of 0.45 mg/mL (n = 3). The Eppendorf tubes containing the PPP and the microspheres, vehicle and the positive/negative controls were incubated at 37 °C with gentle mixing (VWR nutating mixer) for 30 min. After the incubation period, plasma was collected by centrifuging the tubes at 20–22 °C ($2500 \times g$, 10 min). The activated protrombin time (aPTT) was then measured in a Coagulometer (MC10 plus, Merlin medical, Lemgo, Germany). Each sample of PPP (50 μL) was incubated for 3 min at 37 °C, then for 2 min at 37 °C with 50 μL of pre-warmed Activated PTT Reagent, and finally the coagulation was initiated by recalcification with 50 μL pre-warmed 25 mM $CaCl_2$ solution and the coagulation time determined [55]. The clotting time was measured in quadruplo for each sample. Normal coagulations times for the aPTT test should be ≤ 34.1 s [55].

2.2.5.3. Hemolysis. Blood was collected from healthy volunteers and anticoagulated in Lithium heparin tubes (BD Vacutainer® 75 USP units), and the hemolysis assay performed according to the ASTM International standards [56]. Briefly, hemoglobin calibration standards (0.025–0.80 mg/mL) were prepared by dissolving hemoglobin lyophilized powder in cyanmethemoglobin (CMH) reagent. The CMH reagent converts methemoglobin into the CMH form, which is the most stable form of hemoglobin and can then be detected by spectrophotometrically at 540 nm. Quality control samples (0.0625, 0.125 and 0.626 mg/mL) were also prepared to monitor the assay performance by diluting the 0.80 mg/mL hemoglobin calibration standard in CMH reagent. A fraction of the full blood (2 mL) was centrifuged at 20–22 °C ($800 \times g$, 15 min) and the supernatant was collected to determine the plasma-free hemoglobin concentration (PFH) by combining 100 μL of plasma with 100 μL of CMH reagent. The concentration of total blood hemoglobin (TBH) was also determined by combining 20 μL of full blood (not centrifuged) with 5 mL of CMH reagent. The PFH and the TBH in the blood samples of two donors were determined to assess the suitability of the blood and the required blood dilution to perform the assay [56]. The absorbance of the samples PFH, TBH, calibration standards and quality control samples was determined at 540 nm using a plate reader (SpectraMax M2e, Molecular Devices, Canada). The PFH was 0.53 mg/mL (donor 1) and 0.55 mg/mL (donor 2) (requirement is < 1 mg/mL) [56] and the TBH was 220 mg/mL (donor 1) and 195 mg/mL (donor 2) which are both within the normal parameters [56]. Then, the blood samples were diluted with Dulbecco's Phosphate Buffered Saline Ca^{2+}/Mg^{2+}-free (DPBS) to adjust the total blood hemoglobin concentration to 10 ± 2 mg/mL (TBHd). After dilution, the actual TBHd concentration was determined to be 10.3 mg/mL (donor 1) and 9.0 mg/mL (donor 2).

For the analysis of the hemolytic potential of the microspheres, 100 μL of diluted whole blood (TBHd) was added to Eppendorf tubes containing 800 μL of $HoPO_4$-ms or $Ho(OH)_3$-ms suspensions (dispersed in DPBS) at final concentrations of 0.04, 0.2, 1 and 10 mg/mL (n = 3). Suspensions without blood were also prepared by adding solid $HoPO_4$-ms or $Ho(OH)_3$-ms to 900 μL of DPBS at final concentrations of 0.04, 0.2, 1 and 10 mg/mL (n = 3) to detect possible interference from the microspheres in the spectrophotometry determination. As negative control, 800 μL of DPBS was added to 100 μL of diluted whole blood. As positive control, 100 μL of Triton X-100 solution was added to an Eppendorf containing 700 μL of DPBS and 100 μL of diluted whole blood to obtain a final Triton X-100 concentration of 1%. The Eppendorf tubes containing the microspheres with blood, microspheres without blood and the positive/negative controls were incubated at

37 °C with gentle mixing (VWR nutating mixer) for 3 h. Next, the Eppendorf tubes were collected and centrifuged at 20–22 °C ($800 \times g$, 15 min). The concentration of hemoglobin was determined by combining 100 μL of the supernatant with 100 μL of the CMH reagent and measuring the absorbance at 540 nm. Finally, the % hemolysis was calculated using the formula:

$$\% \text{ hemolysis} = \frac{\text{Hemoglobin in test sample}}{\text{TBHd}} \cdot 100\% \qquad (5)$$

The samples after centrifugation were also visually observed to avoid interpretation as false negatives (Fig. S6).

3. Results and discussion

3.1. Preparation and characterization of holmium phosphate (HoPO₄-ms) and holmium hydroxide (Ho(OH)₃-ms) microspheres

Fig. 1-A shows that holmium acetylacetonate microspheres ($Ho_2(AcAc)_3$-ms) developed in previous studies [26,27,50,51] were the starting material to fabricate inorganic microspheres composed of holmium phosphate ($HoPO_4$-ms) and holmium hydroxide ($Ho(OH)_3$-ms). The $Ho_2(AcAc)_3$-ms were suspended in NaH_2PO_4 or NaOH solutions at room temperature for 2 h during which the organic ligands (acetylacetonate) of the $Ho_2(AcAc)_3$-ms were exchanged by phosphate or hydroxyl ions (Fig. 1-B). The formation kinetics of the $HoPO_4$-ms and $Ho(OH)_3$-ms was studied by measuring the concentration of acetylacetone released from the microspheres in the NaH_2PO_4 or NaOH solutions respectively. Figs. S1–A shows that nearly 100% of the acetylacetone originally present in the $Ho_2(AcAc)_3$-ms was released within 45 min of incubation in the 0.58 M NaH_2PO_4 buffer. This measurement reveals that complete exchange of the acetylacetonate by phosphate ions and consequent formation of the $HoPO_4$-ms occurs in less than 1 h.

In the case of the formation of the $Ho(OH)_3$-ms, it was observed that acetylacetone is not stable in the NaOH solution used to prepare the $Ho(OH)_3$-ms. A decrease of acetylacetone concentration after incubation of acetylacetone in a 0.5 M NaOH solution is shown in Figs. S1–B. This instability of acetylacetone in alkaline solutions has been previously assigned to hydrolysis [57]. Due to the hydrolysis of the acetylacetone, the kinetics of acetylacetone released from the $Ho_2(AcAc)_3$-ms during formation of the $Ho(OH)_3$-ms could not be accurately measured. However, measurement of the acetylacetone concentration after 15 min incubation of $Ho_2(AcAc)_3$-ms in the NaOH solution showed that more than 90% of the acetylacetone present in the microspheres was released into the supernatant (Figs. S1–C). This shows that the release of acetylacetone and consequently the formation of $Ho(OH)_3$-ms does rapidly occur within minutes.

Release of acetylacetone upon incubation of $Ho_2(AcAc)_3$-ms in NaH_2PO_4 and NaOH solutions points to the formation of $HoPO_4$-ms and $Ho(OH)_3$-ms respectively. To further prove that inorganic microspheres ($HoPO_4$-ms and $Ho(OH)_3$-ms) were indeed formed, different techniques were applied to characterize the obtained microspheres.

The elemental analysis summarized in Table 1 revealed a drastic alteration of the dried microspheres chemical composition before and after incubation in the NaH_2PO_4 and NaOH solutions. It was observed that the carbon content decreased from 27.2 wt% for the $Ho_2(AcAc)_3$-ms to 0.06 wt% and 0.67 wt% for the $HoPO_4$-ms and $Ho(OH)_3$-ms, respectively. Moreover, the phosphorous content of the $HoPO_4$-ms was determined to be 10.3 wt% and was, as expected, below the detection limit in the $Ho_2(AcAc)_3$-ms and $Ho(OH)_3$-ms. This alteration of the chemical composition of the microspheres resulted in a substantial increase of the holmium weight content from 47.0-47.9 wt% for the $Ho_2(AcAc)_3$-ms to 55.1–55.5 wt% for the $HoPO_4$-ms and even to 72.4–73.1 wt% for the $Ho(OH)_3$-ms.

In order to establish the chemical composition of the microspheres, water molecules were also taken into account. The water content in the $Ho_2(AcAc)_3$-ms had been determined previously using the Karl Fischer

Table 1

Measured and calculated elemental compositions of $Ho_2(AcAc)_3$, $HoPO_4$ and $Ho(OH)_3$ microspheres (in wt %).

Calculated chemical formula	$Ho_2(AcAc)_3$-ms		$HoPO_4$-ms		$Ho(OH)_3$-ms	
	$Ho_2(AcAc)_3 . 2 H_2O$		$HoPO_4 . 2 H_2O$		$Ho(OH)_3 . 0.5 H_2O$	
Element	Calculated	Measured	Calculated	Measured	Calculated	Measured
C[a]	27.0	27.21 ± 0.01	–	0.06 ± 0.00	–	0.67 ± 0.01
H[a]	4.2	4.58 ± 0.01	1.35	1.55 ± 0.01	1.78	1.76 ± 0.01
O[b]	19.2	20.3	32.4	33.0	24.9	24.5
Ho[c]	49.5	47.9 ± 0.01	55.7	55.1 ± 0.02	73.3	73.12 ± 0.01
Ho[d]	49.5	47.0 ± 0.6	55.7	55.5 ± 0.8	73.3	72.4 ± 1.7
P[d]	–	–	10.5	10.3 ± 0.8	–	–

[a] CHNS analyzer.
[b] %O = 100 − (%C + %H + %P + %Ho).
[c] Atomic Absorption Spectroscopy.
[d] Inductively Coupled Plasma - Optical Emission spectroscopy.
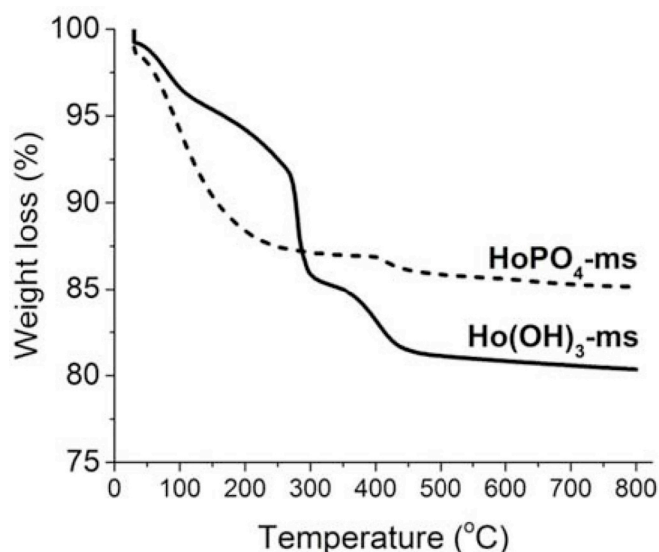
Fig. 2. Thermograms of the $HoPO_4$ and $Ho(OH)_3$ microspheres from 30 to 800 °C performed at heating rate of 5 °C/min under a nitrogen atmosphere.

Fig. 3. Fourier transform infrared (FTIR) spectra of a commercial sample of holmium oxide (Ho_2O_3), and the $HoPO_4$ and $Ho(OH)_3$ microspheres as produced and after heating to 800 °C.

method (5.2 ± 0.7 wt%) [26]. Regarding the $HoPO_4$-ms and $Ho(OH)_3$-ms, it was observed that these microspheres are hygroscopic resulting in an increase of their weight overtime. It was observed that the weight of the $HoPO_4$-ms and the $Ho(OH)_3$-ms increases up to 12 wt% and 9 wt %, respectively, upon storage at 75% relative humidity and 21° for 48 h. Therefore, the measurements of elemental analysis (Table 1) as well as thermogravimetric analysis (TGA) (Fig. 2) were performed after drying the powders overnight in a vacuum oven at 100 °C. The thermograms presented in Fig. 2 of the $HoPO_4$-ms and $Ho(OH)_3$-ms were also acquired after drying of the powders and revealed a weight loss of ~14 wt % for the $HoPO_4$ and a weight loss of ~5 wt% for the $Ho(OH)_3$-ms in the region from 30 to 200 °C. Based on the weight % of the different elements (C, H, P, O and Ho) and the water content after drying, the chemical composition of the different microspheres were calculated (Table 1). The measured elemental composition of the $Ho_2(AcAc)_3$-ms is in agreement with the previously reported chemical formula [26].

The thermal stability of the microspheres up to 800 °C was determined by TGA. Fig. 2 shows that, in the case of the $HoPO_4$-ms, there was a constant weight loss from 30 °C up to approximately 200 °C which is assigned to the loss of water bound to the holmium phosphate complexes. Low weight loss (~2.5 wt%) was observed from 200 up to 800 °C, meaning that the $HoPO_4$-ms are stable at high temperatures. Fig. 3 displays the Fourier-transform infrared (FTIR) spectrum of the $HoPO_4$-ms after heating to 800 °C, which also shows no alteration of the chemical structure of the microspheres.

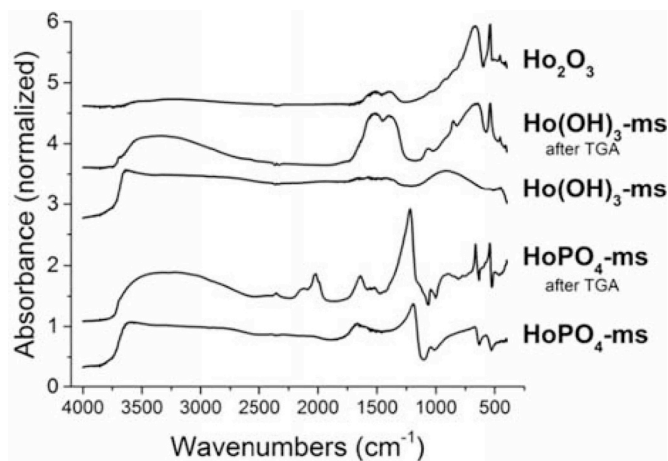The $Ho(OH)_3$-ms lost weight up on heating to 800 °C with two particular weight loss steps of 7.4 ± 0.3 wt% (at 270–300 °C) and 4.0 ± 0.2 wt% (at 350–430 °C) (Fig. 2). This weight loss is assigned to the conversion of $Ho(OH)_3$ into holmium oxide (Ho_2O_3) according to the following reactions: (1) $Ho(OH)_3 \rightarrow HoOOH + H_2O$ (first weight loss step) and (2) $2 HoOOH \rightarrow Ho_2O_3 + H_2O$ (second weight loss step). Similar weight loss behavior has also been observed for the formation of lanthanum oxide from lanthanum hydroxide [58]. Analysis of the $Ho(OH)_3$-ms by FTIR spectroscopy after heating to 800 °C also confirmed the formation of Ho_2O_3 (Fig. 3). The characteristic peaks for the [Ho–O] coordination complexes at 250 to 800 cm^{-1} are detected which corresponds with the presence of Ho_2O_3 [59].

The FTIR spectra displayed in Fig. 3 confirm the composition of the formed inorganic microspheres. The FTIR spectra of the $HoPO_4$-ms showed a distinct peak at 1200 cm^{-1} which corresponds to the [P=O] stretching vibration [59]. In the FTIR spectra of the $Ho(OH)_3$-ms, the hydroxo metal coordination complexes [Ho-OH] were identified at 1200 to 700 cm^{-1} and at 3800 to 3000 cm^{-1} which are attributed to the [O–H] stretching vibration [59]. X-ray powder diffraction analyses showed that both inorganic microspheres were amorphous (Fig. S2) as well as their $Ho_2(AcAc)_3$-ms precursor [26].

In Fig. 4 and Table 2, the size distribution and the mean diameter of the prepared microspheres is presented. The mean diameter of the microspheres decreased after incubation of the $Ho_2(AcAc)_3$-ms in NaH_2PO_4 or NaOH solutions: from 32.6 ± 5.2 μm for the $Ho_2(AcAc)_3$-ms to 28.5 ± 4.4 μm and 25.1 ± 3.5 μm after formation of $HoPO_4$-ms
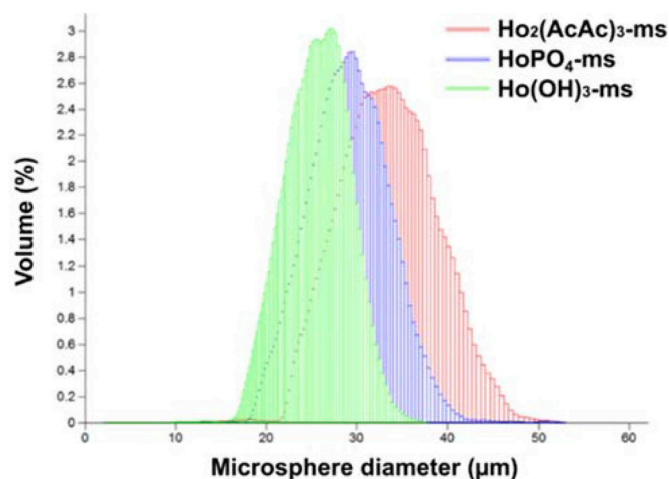
Fig. 4. Size distribution of the $Ho_2(AcAc)_3$, $HoPO_4$ and $Ho(OH)_3$ microspheres.

Table 2
Mean diameter and density of the $Ho_2(AcAc)_3$, $HoPO_4$ and $Ho(OH)_3$ microspheres.

	Diameter (μm)	Density (g/cm^3)
$Ho_2(AcAc)_3$-ms	32.6 ± 5.2	1.7
$HoPO_4$-ms	28.5 ± 4.4	3.0
$Ho(OH)_3$-ms	25.1 ± 3.5	3.6

and $Ho(OH)_3$-ms, which corresponds to a volume shrinkage of 33% and 54% respectively.

Fig. 5 represents scanning electron microscopy and optical microscopy images of the formed microspheres. Despite this major decrease of the microspheres volume, the sphericity and surface smoothness of the prepared microspheres were retained both in the dry state and after suspending in water. Interestingly, a "dot" is observed in the optical microscopy images of the $HoPO_4$-ms (Fig. 5) which points to a different refraction index of the core and the shell of the microspheres and therefore to a different composition. As observed previously, the diameter of the core decreases with incubation time during exchange of the organic ligands (acetylacetonate) by the phosphate ions [26]. Using ImageJ software, the volume percentage contribution of the "dot" was estimated to be only 0.02–0.04% (n = 10), which is considered

minimal. Moreover, the elemental analysis revealed that only traces of C remain present in the $HoPO_4$-ms (0.06 wt%) (Table 1).

Table 2 indicates that the density of the microspheres increased from 1.7 ($Ho_2(AcAc)_3$-ms) to 3.0 ($HoPO_4$-ms) and to 3.6 g/cm^3 (Ho(OH)$_3$-ms) due to both the change in the chemical composition and the decrease of the microspheres size. It has been hypothesized that the density of the microspheres may play a critical role in the distribution of the microspheres in the liver when these are administered in the hepatic artery. The clinically used ^{90}Y microspheres have densities of 1.6 g/cm^3 (SIR-Spheres®) and 3.3 g/cm^3 (TheraSphere®) and the microspheres composed of ^{166}Ho (QuiremSpheres®) have a density of 1.4 g/cm^3 [19]. To date, there is no sufficient clinical data to determine undoubtedly the most appropriate microsphere density for SIRT [60]. Good clinical outcomes have been obtained with microspheres with very distinct densities such as the SIR-Spheres® and TheraSphere® [61–63] and no superior advantage has been undoubtedly attributed to one. Thus, this range of densities appears appropriate for the development of new medical devices for SIRT. The density of the $HoPO_4$-ms and $Ho(OH)_3$-MS is comparable to the clinically used TheraSphere® (3.3 g/cm^3) [19] showing that the inorganic microspheres developed herein can also be potentially used for SIRT of the liver.

The mean zeta potential of the $HoPO_4$-ms was -23.8 ± 8.9 mV and of the $Ho(OH)_3$-ms was -17.9 ± 5.2 mV in water (Fig. 6). This shows that the surface of both microspheres is negatively charged due to the presence of hydroxyl and phosphate ions on the surface of the $HoPO_4$-ms and $Ho(OH)_3$-ms respectively.

3.2. Neutron activation of microspheres

To generate radioactive microspheres, the $HoPO_4$-ms and the $Ho(OH)_3$-ms were exposed to a thermal neutron flux to convert the ^{165}Ho into ^{166}Ho ($^{165}Ho + n \rightarrow ^{166}Ho$, see Table S1). Different amounts of accurately weighted microspheres (254–292 mg) were neutron activated in a nuclear reactor for different times (2, 4 or 6 h). During the neutron activation of the $HoPO_4$-ms, the phosphorous present in the microspheres is converted into radioactive ^{32}P ($^{31}P + n \rightarrow ^{32}P$, see Table S1). After neutron activation, the activity of ^{32}P was approximately 0.02% of the total activity of the activated $HoPO_4$-ms. The reason for this low neutron activation is due to the low thermal neutron cross section of the stable isotope ^{31}P (0.165 barn, Table S1) [64].

After radioactive decay of the activated samples to values of 200–600 MBq/sample (6–8 days after neutron activation), the radioactivity in the samples was measured and used to calculate the activity
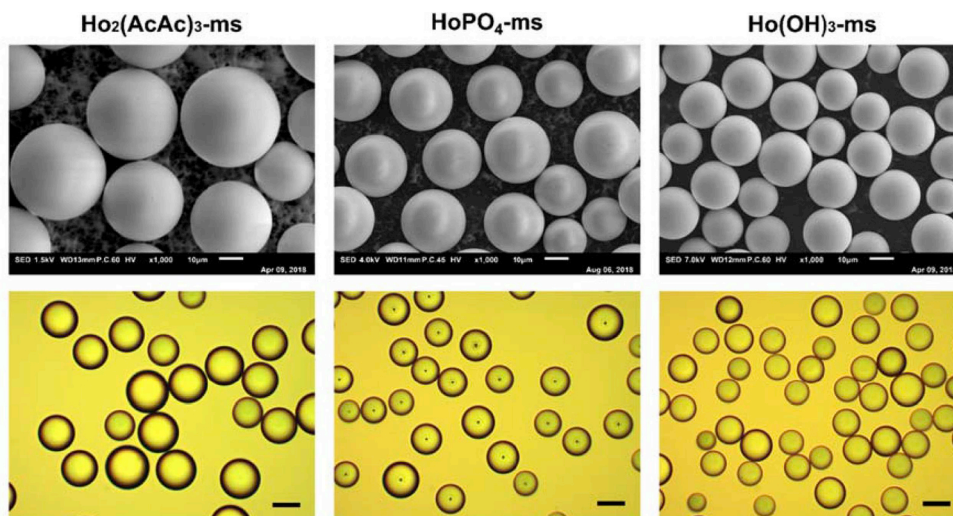

Fig. 5. Scanning electron (top, scale bar 10 μm) and optical (bottom, scale bar 25 μm) microphotographs of holmium acetylacetonate microspheres ($Ho_2(AcAc)_3$-ms), holmium phosphate microspheres ($HoPO_4$-ms) and holmium hydroxide microspheres ($Ho(OH)_3$-ms).

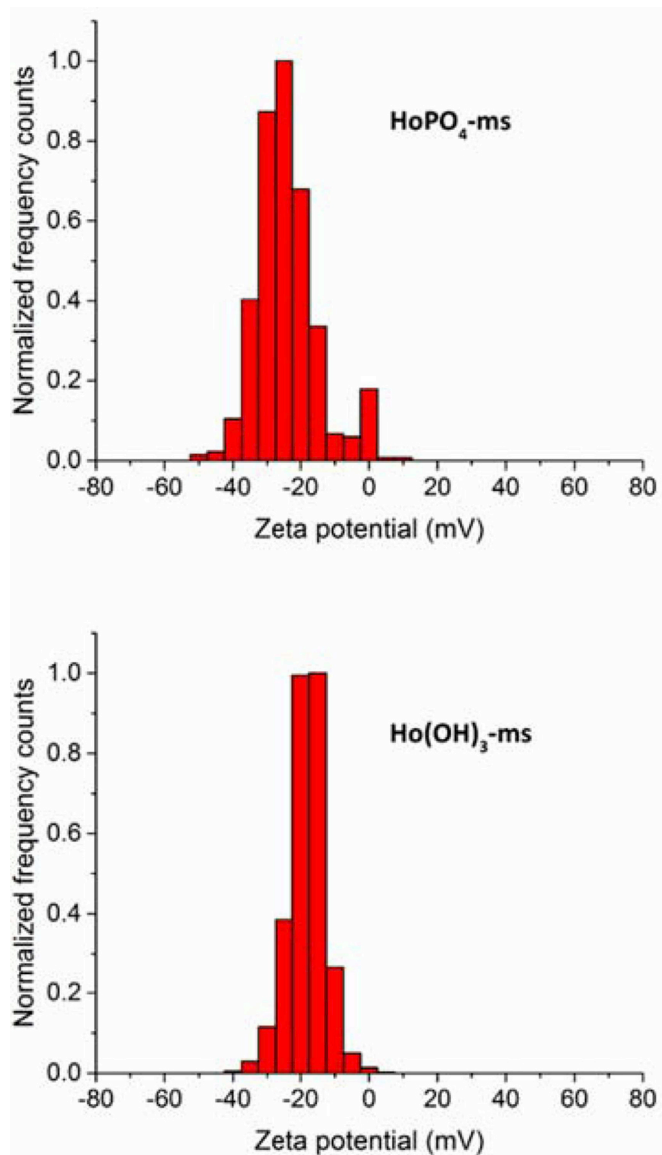**Fig. 6.** Zeta potential of the $HoPO_4$ (top) and $Ho(OH)_3$ (bottom) microspheres in water.
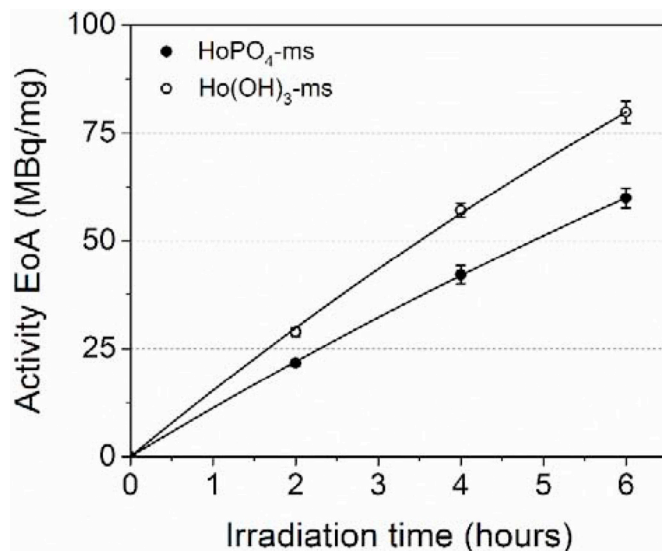

Fig. 7. Specific activities at the end of the activation (EoA) process of $HoPO_4$-ms (●) and $Ho(OH)_3$-ms (○) as a function of the neutron activation time. Masses of microspheres ranged from 254 to 292 mg and neutron activations were performed with an average neutron thermal flux of 4.72×10^{16} n $m^{-2}s^{-1}$.

directly after neutron activation (A_{EoA}) using Equations (3) and (4) (section 2.2.3). Fig. 7 shows that the radioactivity formed depended on the weight percentage of holmium in the samples - $HoPO_4$-ms (55 wt%) and $Ho(OH)_3$-ms (73 wt%). Thus, the $Ho(OH)_3$-ms generated higher activities than the $HoPO_4$-ms when activated under the same conditions.

The $HoPO_4$-ms generated specific activities ranging from 21.7-59.9 MBq/mg (Fig. 7), which correspond to total activities from 6.0 to 16.7 GBq/sample when neutron activating approximately 275 mg of sample. The specific activities formed after neutron activation of the $Ho(OH)_3$-ms ranged from 28.8-79.9 MBq/mg (Fig. 7), corresponding to total activities from 7.2 to 20.9 GBq/sample when neutron activating approximately 275 mg of $Ho(OH)_3$-ms.

From these results, one can determine the specific activity in MBq per individual microsphere (MBq/microsphere) using the total number of microspheres per sample which was calculated using the microsphere's density and their mean diameter (Table 2). The specific activity per microsphere was 767–2261 Bq/microsphere for the $HoPO_4$-ms and 828–2451 Bq/microsphere for the $Ho(OH)_3$-ms. The polymeric ^{166}Ho-PLA-ms used in the clinics (QuiremSpheres®) have a specific activity of

450 Bq/microsphere [19]. The range of activities obtained for the $HoPO_4$-ms and for the $Ho(OH)_3$-ms are therefore 1.7–5.5 times higher than the activities of the systems used in the clinics for SIRT of liver malignancies with ^{166}Ho.

The higher specific activity of these newly developed microspheres provides several potential advantages for their target applications. For example, it allows to decrease the amount of microspheres administered per treatment which can be beneficial for SIRT. In SIRT, the use of too many microspheres will result in backflow and filling of the normal healthy liver tissue, while a lower amount of microspheres will reduce the risk of stasis and particle reflux [19]. Thus, these microspheres can be adapted to the patient needs enabling fine tuning between the treatment dose and the number of microspheres administered. Likewise, the higher specific activity allows the use of these microspheres as a "scout dose" which betters predict the microsphere's distribution during the treatment dose and avoids unwanted extrahepatic deposition of the microspheres, as it is currently being successfully performed with the ^{166}Ho-PLA-ms (QuiremScout®) [43,48].

Furthermore, the higher specific activity of the microspheres developed herein makes them especially interesting for intratumoral applications. For intratumoral injection, there is often a limited space because the microspheres are injected interstitially and therefore lowering the amount of microspheres can be advantageous to avoid increase of the tumor interstitial fluid pressure [14,49,65].

3.3. Stability of microspheres after neutron activation

The shelf-life stability of neutron activated $HoPO_4$-ms and $Ho(OH)_3$-ms was tested after a decay time of more than 20 days by incubation of the microspheres in administration fluids suitable for SIRT. The radiation dose received by the microspheres originated from the (a) reactor environment during neutron activation (depended on the neutron activation time), and from the (b) decay of the formed isotope ^{166}Ho (internal radiation dose) which varied per sample according to the ^{166}Ho activity generated (Fig. 7). The decay time of 20 days ensured that the microspheres received the maximum level of internal radiation dose for each tested condition in order to simulate the worst-case scenario.

Prior to testing of the neutron activated microspheres, the stability

of non-radioactive $HoPO_4$-ms and $Ho(OH)_3$-ms was studied in sodium phosphate buffer (0.116 M, pH 7.2) and saline (0.9% NaCl) solutions respectively (Fig. S3), which are both suitable vehicles for intravenous use [66]. It was observed that the $HoPO_4$-ms were well dispersed in 0.116 M phosphate buffer but show agglomeration in the 0.9% NaCl solution (Fig. S3). In the case of the $Ho(OH)_3$-ms, improved dispersion stability was observed in the 0.9% NaCl solution, whereas signs of agglomeration were observed in the 0.116 M phosphate buffer solution (Fig. S3). Given the good stability of the $HoPO_4$-ms and the $Ho(OH)_3$-ms before neutron activation in 0.116 M phosphate buffer and 0.9% NaCl respectively, the stability of the radioactive microspheres was tested in the same solutions. Both radioactive microspheres remained spherical and no signs of agglomeration were observed in the administration fluids (Fig. S4). Table S2 shows that the mean diameter and the volume % of microspheres in the range 15–50 μm did not change significantly. Moreover, the holmium released from the microspheres was very low up to 72 h incubation in the solutions (< 0.05%). These results demonstrate that the neutron activated $HoPO_4$-ms and $Ho(OH)_3$-ms are very stable after neutron activation and dispersion in the administration fluids for at least 72 h.

The stability of these microspheres to long neutron activation times (at least 6 h in a neutron flux of 4.72×10^{16} neutrons $m^{-2} s^{-1}$) together with their long-term stability in suspension fluids (at least 72 h) makes them particularly advantageous in terms of product logistics. The high stability to neutron activation and long shelf-life allows to increase the time for sample transportation which simplifies the logistics handling of the products from the neutron activation facility (nuclear reactor) to the hospital site.

3.4. Hemocompatibility

The use of these inorganic microspheres as a medical device for internal radionuclide therapy requires several biocompatibility tests to assess whether their use in humans is safe. One of the requirements of microspheres that will directly contact blood in certain applications such as radiation segmentectomy or SIRT [6–8] is that they have a good hemocompatibility. In this work, three hemocompatibility tests were performed.

The first test was incubation of microspheres (concentrations from 5 to 40 mg/mL) with full blood followed by analysis of the hemogram after 4 and 24 h (Fig. S5 and Fig. 8-A). Statistical analysis of the hemogram results revealed no statistically significant difference between the blood incubated with the microspheres and the respective controls (p > 0.05). These results show that the $HoPO_4$-ms and $Ho(OH)_3$-ms did not induce alterations of the blood parameters (Fig. S5). Moreover, Fig. 8-A shows that no statistically significant cytotoxicity was observed towards the white blood cells.

The second hemocompatibility parameter analyzed was the potential of the microspheres to interact with blood coagulation factors. Undesirable activation of blood clotting may lead to the formation of a thrombus that can result in the partial or complete occlusion of a blood vessel and ultimately in a life-threatening condition such as stroke [55]. Alternatively it is highly undesirable that coagulation factors adsorb onto the surface of blood contacting medical devices which might lead to depletion of the factors from the circulations. There are different tests to determine the potential of a foreign material to induce blood clotting via the intrinsic (contact activation pathway), extrinsic (tissue factor
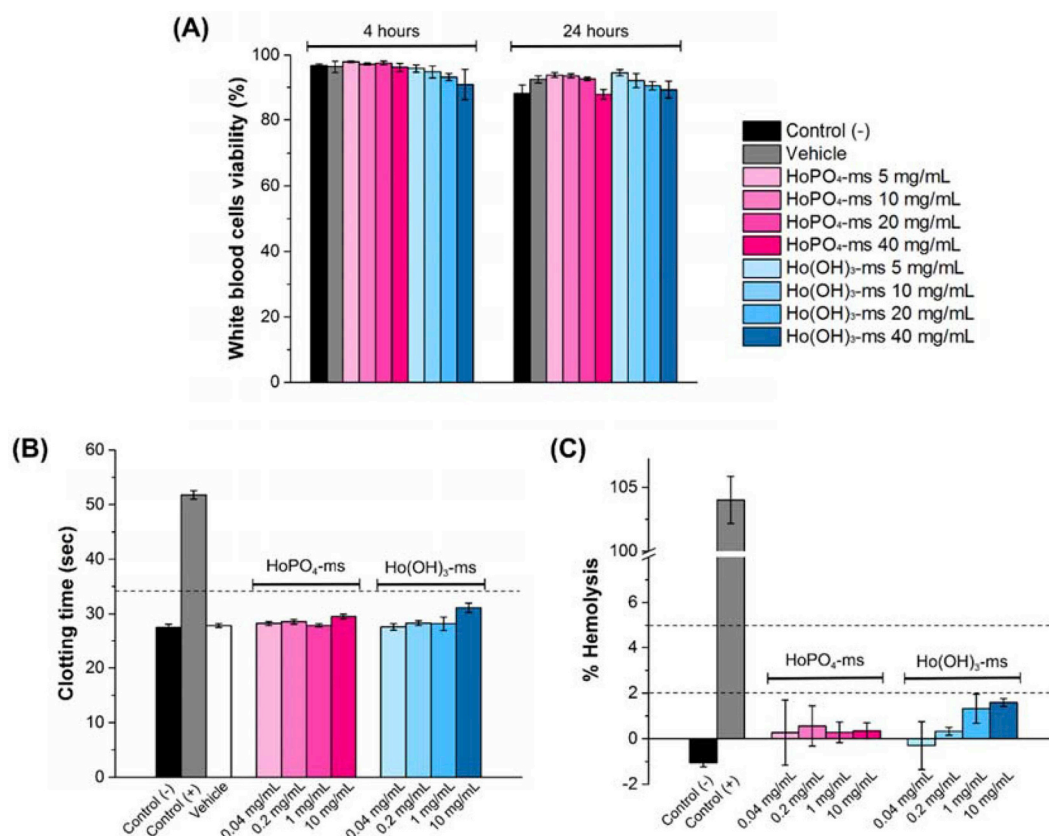

Fig. 8. Hemocompatibility of $HoPO_4$ and $Ho(OH)_3$ microspheres. (A) Viability of white blood cells after incubation of full blood with the microspheres for 4 and 24 h at 37 °C. (B) Clotting time (aPTT test) of human plasma after incubation of human plasma with the microspheres for 30 min at 37 °C: clotting times above dash line (> 34.1 s) are considered abnormal. (C) The % of hemolysis after incubation of diluted human blood with the microspheres for 3 h at 37 °C. < 2% hemolysis sample is not-hemolytic, 2–5% sample is slightly hemolytic, and > 5% sample is hemolytic [56].

pathway) and the common pathways. In this work, the ability of the $HoPO_4$-ms and $Ho(OH)_3$-ms to interact with the plasma coagulation factors of the intrinsic pathway was assessed using the activated pro-thrombin time (aPTT) test [55]. This assay evaluates the functionality of some coagulation factors (XII, XI, IX, VIII, X, V and II) and an in-crease of the coagulation time suggests that the materials deplete or inhibit these coagulation factors [55]. Therefore, a plasma coagulation time longer than the normal value for the aPTT test (> 34.1 s) is considered abnormal. For this test, microspheres were incubated with human plasma and the coagulation times after incubation with the aPTT reagent were measured. Fig. 8-B shows that neither the $HoPO_4$-ms nor the $Ho(OH)_3$-ms deplete or inhibit the coagulation factors of the intrinsic pathway in the concentration range tested (0.04–10 mg/mL) [55]. The positive control plasma was exposed to a known blood clot activator (kaolin) [67] which resulted in an increase of the aPTT clot-ting time (Fig. 8-B) above the maximum limit of 34.1 s [55], suggesting that the coagulation factors adsorbed onto the kaolin surface depleting them from plasma.

Thirdly, the hemolysis potential of the $HoPO_4$-ms and $Ho(OH)_3$-ms was determined upon their incubation with diluted human heparinized blood. Hemolysis can lead to anemia and other serious pathological conditions as extracellular hemoglobin is toxic and may affect vascular, myocardial, renal and central nervous system tissues [56]. The results expressed as percent of hemolysis (Fig. 8-C) were used to evaluate the acute *in vitro* hemolytic properties of the microspheres. A sample with a % of hemolysis < 2% is considered not hemolytic, a % of hemolysis between 2 and 5 is considered slightly hemolytic, and a result > 5% means the sample is hemolytic according to the ASTM International standards [56]. Fig. S6 shows photographs of the testing tubes, which were collected to avoid misinterpretation of the results as false nega-tives. The results displayed in Fig. 8-C demonstrate that the $HoPO_4$-ms and the $Ho(OH)_3$-ms are not hemolytic in the concentration range tested (0.04–10 mg/mL).

4. Conclusions

This study shows that $HoPO_4$-ms and $Ho(OH)_3$-ms are formed upon incubation of $Ho_2(AcAc)_3$-ms with NaH_2PO_4 or NaOH solutions at room temperature. After neutron activation of the $HoPO_4$-ms and $Ho(OH)_3$-ms, the microspheres achieved specific activities ranging from 21.7-59.9 MBq/mg for the $HoPO_4$-ms and 28.8–79.9 MBq/mg for the $Ho(OH)_3$-ms. The specific activity can be tuned by adjusting the neutron activation time according to the individual patient dosing requirement, medical application of microspheres or transportation needs. The mi-crospheres were capable of withstanding prolonged neutron activation periods (up to 6 h at a neutron flux of 4.72×10^{16} n m^{-2}s^{-1}) and showed excellent stability in appropriate administration fluids for at least 72 h. The developed production and neutron activation methods are considered feasible for the commercial production of therapeutic ^{166}Ho loaded inorganic microspheres. Importantly it was shown that the microspheres have an excellent hemocompatibility. It is concluded that the inorganic ^{166}HoPO$_4$-ms and ^{166}Ho(OH)$_3$-ms radioactive mi-crospheres are both potential candidates for application in internal radionuclide therapy of malignancies. Future research will focus on the imaging capabilities (MRI/SPECT/CT) and on preclinical testing of these new microspheres.

Declaration of competing interest

Dr. JFW Nijsen is inventor on the patents related to the $Ho_2(AcAc)_3$-ms and $HoPO_4$-ms which are assigned to University Medical Center Utrecht Holding BV and/or Quirem Medical (patent families: USA Patent No. 6,373,068 B1, PCT/NL03/00485, EP07112807.8, 10190254.2, P114198PC00, P112614NL00). He is co-founder and chief scientific officer of Quirem Medical, and has a minority share in the company Quirem Medical. The activities of F.W. Nijsen within Quirem

Medical are approved and supported by Prof. Dirkjan Masman (Director Technology Transfer Office Radboudumc) and Prof. dr. Mathias Prokop (Head of Radiology and Nuclear Medicine at Radboudumc). All authors have revised and approved the final manuscript.

Appendix A. Supplementary data

Supplementary data to this article can be found online at https://doi.org/10.1016/j.msec.2019.110244.

References

[1] I. Soerjomataram, J. Lortet-Tieulent, D.M. Parkin, J. Ferlay, C. Mathers, D. Forman, F. Bray, Lancet 380 (2012) 1840–1850.
[2] L.R. Zarour, S. Anand, K.G. Billingsley, W.H. Bisson, A. Cercek, M.F. Clarke, L.M. Coussens, C.E. Gast, C.B. Geltzeiler, L. Hansen, K.A. Kelley, C.D. Lopez, S.R. Rana, R. Ruhl, V.L. Tsikitis, G.M. Vaccaro, M.H. Wong, S.C. Mayo, Cell. Mol. Gastroenterol. Hepatol. 3 (2017) 163–173.
[3] S.F. Altekruse, K.A. McGlynn, M.E. Reichman, J. Clin. Oncol. 27 (2009) 1485–1491.
[4] J. Ferlay, I. Soerjomataram, R. Dikshit, S. Eser, C. Mathers, M. Rebelo, D.M. Parkin, D. Forman, F. Bray, Int. J. Cancer 136 (2015) 9.
[5] E.P. Misiakos, N.P. Karidis, G. Kouraklis, World J. Gastroenterol. 17 (2011) 4067–4075.
[6] C. Meiers, A. Taylor, B. Geller, B. Toskich, J. Gastrointest. Oncol. 9 (2018) 311–315.
[7] F.E. Boas, L. Bodei, C.T. Sofocleous, J. Nucl. Med. 58 (2017) 187229.
[8] J.F. Prince, M. van den Bosch, J.F.W. Nijsen, M.L.J. Smits, A.F. van den Hoven, S. Nikolakopoulos, F.J. Wessels, R.C.G. Bruijnen, M. Braat, B.A. Zonnenberg, M. Lam, J. Nucl. Med. 15 (2017) 197194.
[9] B. Sangro, M. Iñarrairaegui, J.I. Bilbao, J. Hepatol. 56 (2012) 464–473.
[10] D. Coldwell, B. Sangro, H. Wasan, R. Salem, A. Kennedy, Am. J. Clin. Oncol. 34 (2011) 337–341.
[11] S. Ho, W.Y. Lau, T.W. Leung, P.J. Johnson, Cancer 83 (1998) 1894–1907.
[12] N. Firusian, W. Dempke, Cancer 85 (1999) 980–987.
[13] J.K. Kim, K.H. Han, J.T. Lee, Y.H. Paik, S.H. Ahn, J.D. Lee, K.S. Lee, C.Y. Chon, Y.M. Moon, Clin. Cancer Res. 12 (2006) 543–548.
[14] R.C. Bakker, M.G.E.H. Lam, S.A. van Nimwegen, A.J.W.P. Rosenberg, R.J.J. van Es, J.F.W. Nijsen, J. Radiat. Oncol. 6 (2017) 323–341.
[15] C. Rognoni, O. Ciani, S. Sommariva, A. Facciorusso, R. Tarricone, S. Bhoori, V. Mazzaferro, Oncotarget 7 (2016) 72343–72355.
[16] M.S. Dendy, J.M. Ludwig, H.S. Kim, Oncotarget 8 (2017) 37912–37922.
[17] V.M. Meade, M.A. Burton, B.N. Gray, G.W. Self, Eur. J. Cancer Clin. Oncol. 23 (1987) 37–41.
[18] J.H. Anderson, W.J. Angerson, N. Willmott, D.J. Kerr, C.S. McArdle, T.G. Cooke, Br. J. Canc. 64 (1991) 1031–1034.
[19] A. Pasciak, Handbook of Radioembolization, CRC Press, Taylor & Francis Group, LLC, 2017.
[20] E. Lanza, M. Donadon, D. Poretti, V. Pedicini, M. Tramarin, M. Roncalli, H. Rhee, Y.N. Park, G. Torzilli, Liver Canc. 6 (2016) 27–33.
[21] H.-C. Kim, Clin. Mol. Hepatol. 23 (2017) 109–114.
[22] J.F. Nijsen, A.D. van het Schip, W.E. Hennink, D.W. Rook, P.P. van Rijk, J.M. de Klerk, Curr. Med. Chem. 9 (2002) 73–82.
[23] W. Lada, E. Iller, D. Wawszczak, M. Konior, T. Dziel, Mater. Sci. Eng. C 67 (2016) 629–635.
[24] M. Kawashita, Mater. Sci. Eng. C 22 (2002) 3–8.

[25] D. Zhao, W. Huang, M.N. Rahaman, D.E. Day, D. Wang, Y. Gu, Mater. Sci. Eng. C 32 (2012) 276–281.
[26] A.G. Arranja, W.E. Hennink, A.G. Denkova, R.W.A. Hendrikx, J.F.W. Nijsen, Int. J. Pharm. 548 (2018) 73–81.
[27] W. Bult, P.R. Seevinck, G.C. Krijger, T. Visser, L.M.J. Kroon-Batenburg, C.J.G. Bakker, W.E. Hennink, A.D. van het Schip, J.F.W. Nijsen, Pharm. Res. 26 (2009) 1371–1378.
[28] A.S. Goh, A.Y. Chung, R.H. Lo, T.N. Lau, S.W. Yu, M. Chng, S. Satchithanantham, S.L. Loong, D.C. Ng, B.C. Lim, S. Connor, P.K. Chow, Int. J. Radiat. Oncol. Biol. Phys. 67 (2007) 786–792.
[29] C.-C. Li, J.-L. Chi, Y. Ma, J.-H. Li, C.-Q. Xia, L. Li, Z. Chen, X.-L. Chen, Radiat. Oncol. 9 (2014) 144-144.
[30] S.J. Wang, W.Y. Lin, M.N. Chen, C.S. Chi, J.T. Chen, W.L. Ho, B.T. Hsieh, L.H. Shen, Z.T. Tsai, G. Ting, S. Mirzadeh, F.F. Knapp Jr., J. Nucl. Med. 39 (1998) 1752–1757.
[31] QuiremSpheres®, https://www.quirem.com/quiremspheres/.
[32] SIR-Spheres®, http://sirtex.com/.
[33] TheraSphere®, http://btgplc.com/TheraSphere/.
[34] J.H. Seppenwoolde, J.F. Nijsen, L.W. Bartels, S.W. Zielhuis, A.D. van Het Schip, C.J. Bakker, Magn. Reson. Med. 53 (2005) 76–84.
[35] M.L. Smits, M. Elschot, M.A. van den Bosch, G.H. van de Maat, A.D. van het Schip, B.A. Zonnenberg, P.R. Seevinck, H.M. Verkooijen, C.J. Bakker, H.W. de Jong, M.G. Lam, J.F. Nijsen, J. Nucl. Med. 54 (2013) 2093–2100.
[36] P.R. Seevinck, J.H. Seppenwoolde, T.C. de Wit, J.F. Nijsen, F.J. Beekman, A.D. van Het Schip, C.J. Bakker, Anti Cancer Agents Med. Chem. 7 (2007) 317–334.
[37] J.F. Nijsen, J.H. Seppenwoolde, T. Havenith, C. Bos, C.J. Bakker, A.D. van het Schip, Radiology 231 (2004) 491–499.
[38] J.F.W. Nijsen, M.J. van Steenbergen, H. Kooijman, H. Talsma, L.M.J. Kroon-Batenburg, M. van de Weert, P.P. van Rijk, A. de Witte, A.D. van het Schip, W.E. Hennink, Biomaterials 22 (2001) 3073–3081.
[39] S.W. Zielhuis, J.F. Nijsen, R. de Roos, G.C. Krijger, P.P. van Rijk, W.E. Hennink, A.D. van het Schip, Int. J. Pharm. 311 (2006) 69–74.
[40] M. Elschot, M.L. Smits, J.F. Nijsen, M.G. Lam, B.A. Zonnenberg, M.A. van den Bosch, M.A. Viergever, H.W. de Jong, Med. Phys. 40 (2013) 4823788.
[41] M. Elschot, J.F. Nijsen, A.J. Dam, H.W. de Jong, PLoS One 6 (2011) 3.
[42] G.H. van de Maat, P.R. Seevinck, C. Bos, C.J. Bakker, J. Magn. Reson. Imaging 35 (2012) 1453–1461.
[43] QuiremScout®, https://www.quirem.com/quiremscout/.
[44] J.F. Prince, R. van Rooij, G.H. Bol, H.W. de Jong, M.A. van den Bosch, M.G. Lam, J. Nucl. Med. 56 (2015) 817–823.
[45] M. Elschot, J.F. Nijsen, M.G. Lam, M.L. Smits, J.F. Prince, M.A. Viergever, M.A. van den Bosch, B.A. Zonnenberg, H.W. de Jong, Eur. J. Nucl. Med. Mol. Imag. 41 (2014) 1965–1975.
[46] M. Wondergem, M.L. Smits, M. Elschot, H.W. de Jong, H.M. Verkooijen, M.A. van den Bosch, J.F. Nijsen, M.G. Lam, J. Nucl. Med. 54 (2013) 1294–1301.
[47] M.A.D. Vente, T.C. de Wit, M.A.A.J. van den Bosch, W. Bult, P.R. Seevinck, B.A. Zonnenberg, H.W.A.M. de Jong, G.C. Krijger, C.J.G. Bakker, A.D. van het Schip, J.F.W. Nijsen, Eur. Radiol. 20 (2010) 862–869.
[48] M.L.J. Smits, M.G. Dassen, J.F. Prince, A.J.A.T. Braat, C. Beijst, R.C.G. Bruijnen, H.W.A.M. de Jong, M.G.E.H. Lam, European Journal of Nuclear Medicine and Molecular Imaging, (2019).
[49] S.A. van Nimwegen, R.C. Bakker, J. Kirpensteijn, R.J.J. van Es, R. Koole, M. Lam, J.W. Hesselink, J.F.W. Nijsen, Vet. Comp. Oncol. 8 (2017) 12319.
[50] W. Bult, H. de Leeuw, O.M. Steinebach, M.J. van der Bom, H.T. Wolterbeek, R.M.A. Heeren, C.J.G. Bakker, A.D. van het Schip, W.E. Hennink, J.F.W. Nijsen, Pharm. Res. 29 (2012) 827–836.
[51] W. Bult, J.F. Nijsen, A.D. van het Schip, A microsphere comprising an organic lanthanide metal complex, 2007, patent number EP07112807.8.
[52] J.F.W. Nijsen, B.A. Zonnenberg, J.R.W. Woittiez, D.W. Rook, I.A. Swildens-van Woudenberg, P.P. van Rijk, A.D. van het Schip, Eur. J. Nucl. Med. 26 (1999) 699–704.
[53] R.J. Hunter, Zeta Potential in Colloid Science, Academic Press, 2013.
[54] M.A. Vente, J.F. Nijsen, R. de Roos, M.J. van Steenbergen, C.N. Kaaijk, M.J. Koster-Ammerlaan, P.F. de Leege, W.E. Hennink, A.D. van Het Schip, G.C. Krijger, Biomed. Microdevices 11 (2009) 763–772.
[55] T.M. Potter, J.C. Rodriguez, B.W. Neun, A.N. Ilinskaya, E. Cedrone, M.A. Dobrovolskaia, In vitro assessment of nanoparticle effects on blood coagulation, in: S.E. McNeil (Ed.), Characterization of Nanoparticles Intended for Drug Delivery, Springer New York, New York, NY, 2018, pp. 103–124.
[56] B.W. Neun, A.N. Ilinskaya, M.A. Dobrovolskaia, Updated method for in vitro analysis of nanoparticle hemolytic properties, Characterization of Nanoparticles Intended for Drug Delivery, 2018 7352-7351_7359.
[57] R.G. Pearson, A.C. Sandy, J. Am. Chem. Soc. 73 (1951) 931–934.
[58] A. Neumann, D. Walter, Thermochim. Acta 445 (2006) 200–204.
[59] G. Socrates, Infrared and Raman Characteristic Group Frequencies : Tables and Charts, third ed., Wiley, Chichester ; New York, 2001.
[60] M.A. Westcott, D.M. Coldwell, D.M. Liu, J.F. Zikria, Adv. Radiat. Oncol. 1 (2016) 351–364.
[61] S.M. Srinivas, E.C. Nasr, V.K. Kunam, J.A. Bullen, A.S. Purysko, J. Gastrointest. Oncol. 7 (2016) 530–539.
[62] N.P. Burnett, O. Akinwande, C.R. Scoggins, K.M. McMasters, P. Philips, R.C. Martin, J. Radiat. Oncol. 6 (2017) 101–108.
[63] A. Van Der Gucht, M. Jreige, A. Denys, P. Blanc-Durand, A. Boubaker, A. Pomoni, P. Mitsakis, M. Silva-Monteiro, S. Gnesin, M.N. Lalonde, R. Duran, J.O. Prior, N. Schaefer, J. Nucl. Med. 58 (2017) 1334–1340.
[64] L. Seren, H.N. Friedlander, S.H. Turkel, Phys. Rev. 72 (1947) 888–901.
[65] R.C. Bakker, R.J.J. van Es, A. Rosenberg, S.A. van Nimwegen, R. Bastiaannet, H. de Jong, J.F.W. Nijsen, M. Lam, Nucl. Med. Commun. 39 (2018) 213–221.
[66] R. Rowe, P. Sheskey, S. Owen, Handbook of Pharmaceutical Excipients, Pharmaceutical Press, 2006.
[67] C. Haanen, Human Blood Coagulation: Biochemistry, Clinical Investigation and Therapy, Leiden University Press, Leiden, 1969.